AIAA JOURNAL
Vol. 46, No. 7, July 2008

Flow Relaxation Past a Transverse Square Rib in Pressure Gradients

Mohammad K. Shah* and Mark F. Tachie†
University of Manitoba, Winnipeg, Manitoba, R3T 5V6, Canada

DOI: 10.2514/1.35528

An experimental investigation is undertaken to study the salient features of separated and reattached flows over a transverse square rib in an asymmetric diverging and converging channel. To facilitate comparison, experiments were also performed in a parallel-walled channel for which the pressure gradient is nearly zero. The transverse square rib was located 1000 mm from the inlet of a given channel (at the inlet to the convergence/divergence section). A high-resolution particle image velocimetry was used to conduct the velocity measurements. From these measurements, isocontour plots of mean velocity, Reynolds shear stress, and spanwise vorticity in the vicinity of the rib were reported. The profiles of mean velocities, Reynolds stresses, triple products, and some of the terms in the transport equations for turbulent kinetic energy and Reynolds shear stress are reported in the separated and redevelopment regions as far downstream as 200 step heights.

I. Introduction

FLOW separation induced by obstacles occurs in diverse practical engineering applications. For example, pipe systems in chemical reactors or food-processing devices may have abrupt changes in tube diameter or may be furnished with baffles or ribs that obstruct the flow. Similarly, flows over and around wall-mounted obstacles or through orifices are frequently encountered in practice: for example, with heat exchangers and combustors. Turbulent flow separation and subsequent reattachment also occurs in aerodynamics: for example, in flow over an airfoil. In these and many other applications, the characteristics of separation and reattachment of the flow may significantly affect the efficiency and performance of the fluid engineering devices. Apart from their practical engineering importance, separated and reattached turbulent flows are used as prototypical flows to advance understanding of complex near-wall turbulence.

A number of laboratory geometries or obstacles have been devised to generate two-dimensional separated and reattached flows. These geometries include a backward-facing step (Bradshaw and Wong [1]), a forward-facing step (Abu-Mulaweh [2]), a transverse square rib (Abdalla et al. [3]), a splitter plate (Ruderich and Fernholz [4]), and a blunt plate (Kiya and Sasaki [5]). Irrespective of the specific geometry, the flowfield can be divided into two regions: 1) the separated/recirculating region and 2) the recovery/redevelopment region. Figure 1 depicts these regions and also defines some of the flow nomenclature for a two-dimensional transverse square rib. As shown in the figure, the separated region spans from the point of separation to the location at which the flow reattaches onto the floor, and the region downstream of the reattachment region is called the redevelopment region. The separated flow downstream of the rib causes recirculation that is often referred to as the separation bubble. The mean reattachment length x_r is the distance between the location of separation and the reattachment point.

The salient features of separated and reattached flows past an obstacle are well documented in the literature. A summary of selected previous experimental studies conducted in zero-pressure-gradient (ZPG) boundary layers, parallel-walled closed channels (CC), open channels (OC), an adverse pressure gradient (APG), and a favorable pressure gradient (FPG) is provided by Shah and Tachie [6]. The quantities reported in those studies include the pressure coefficient C_p, reattachment length x_r, displacement thickness δ^*, momentum thickness θ, streamwise mean velocity U, turbulent intensities u', v', and w', Reynolds stresses $\langle u^2\rangle$, $\langle v^2\rangle$, $\langle w^2\rangle$, and $\langle -uv\rangle$, turbulent kinetic energy, and triple correlations $\langle u^3\rangle$, $\langle u^2v\rangle$, $\langle uv^2\rangle$, $\langle v^3\rangle$, $\langle u^2w\rangle$, $\langle uw^2\rangle$, and $\langle w^3\rangle$. The complete terms in the transport equation for the turbulent kinetic energy equation are reported in a few studies (Castro and Epik [7] and Piirto et al. [8]). The hot-wire and laser Doppler anemometry (LDA) were used in most of the previous experiments. It should be noted that in spite of their excellent spatial and temporal resolutions, the LDA and hot wire provide pointwise measurement, and so it is a challenging undertaking to measure some of the terms in the transport equations for the turbulent kinetic energy and Reynolds stresses. This is particularly true within and immediately downstream of the recirculating region, in which the flow evolves rapidly in the streamwise direction. The presence of flow reversal and high local turbulence levels within the recirculation region also preclude the use of standard hot wires to accurately measure the velocity field in the recirculation region. Although the particle image velocimetry (PIV) technique cannot match the temporal resolution obtainable from the hot wire, it is a whole-field measurement technique and is therefore well suited for estimating velocity gradients and derived quantities such as vorticity and the various terms in the transport equations for turbulent kinetic energy and Reynolds stresses.

Previous studies have shown that the Reynolds number, blockage ratio, and aspect ratio (the ratio of obstacle length to obstacle height) are some of the parameters that affect the flow characteristics over an obstacle. Bergeles and Athanassiadis [9] investigated the effect of obstacle aspect ratio on the mean reattachment length. They reported that for obstacle widths smaller than $4k$ (k is the rib height), the shear layer separating from the upstream edge reattaches past the obstacle and the reattachment length decreases linearly with the obstacle width. Jović [10] investigated the flow recovery downstream of a backward-facing step for five different flow conditions by varying k and Re_k while keeping the blockage ratio in a narrow range of 0.04–0.09. It was found that the reattachment length increased from 5.35 to 6.94 as the Re_k increased from 6800 to 37,200. The inner region of the boundary layer was observed to recover to an equilibrium state at $x = 15k$ ($Re_k > 25,500$) and sooner for lower Re_k cases. Djilali and Gartshore [11] compiled values of x_r obtained from different studies and concluded that x_r decreases with increasing solid blockage ratio, defined as the ratio of the obstacle height to the channel or

Received 6 November 2007; revision received 3 April 2008; accepted for publication 6 April 2008.

*Graduate Student, Mechanical and Manufacturing Engineering Department, 75A Chancellors Circle. Student Member AIAA.

†Associate Professor, Mechanical and Manufacturing Engineering Department, 75A Chancellors Circle. Member AIAA.

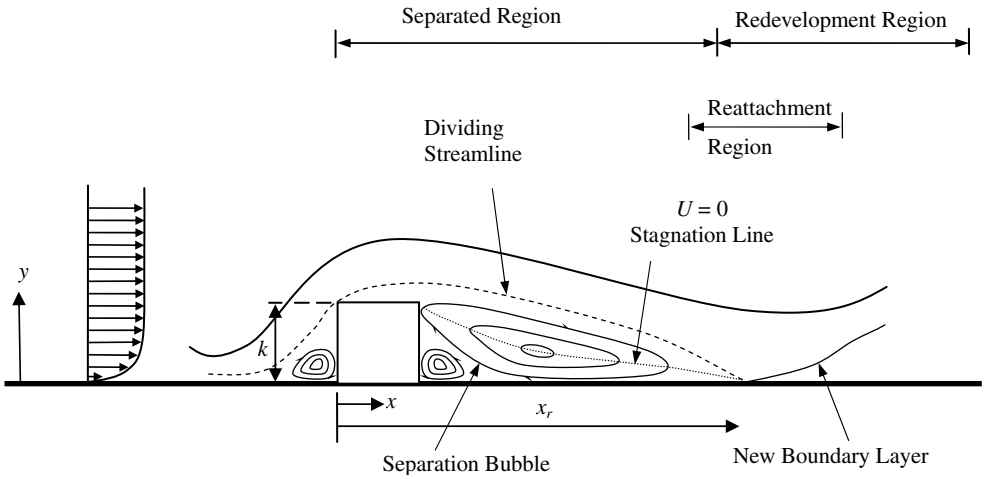

Fig. 1 Flow regions downstream of a rib.

wind-tunnel height. A study of forward-facing step flow was conducted by Abu-Mulaweh [2] to explore the effects of step height. The results show that as the step height increases, so do the reattachment length and velocity fluctuations.

Only a few studies to date have investigated the characteristics of separated and reattached flows downstream of an obstacle in the presence of an APG or FPG. Cutler and Johnston [12] employed a hot wire and pitot tube to study the relaxation of a reattached turbulent boundary layer downstream of a wall fence in an APG. The pressure gradient imposed on the turbulent boundary layer was adjusted by means of a nonlinearly curved roof to keep the boundary layer in equilibrium. In their study, the flow reattached upstream of the divergence and results were presented downstream of the reattachment location up to 83 step heights. They reported that the results downstream of reattachment were qualitatively similar to the ZPG boundary-layer data of Driver and Seegmiller [13] and Kim et al. [14]. Kuehn [15] reported the reattachment length and mean velocity in the redevelopment region of a backward-facing step in which the roof immediately downstream of the backward-facing step was tilted at various angles in the range of $-10\,\text{deg} \leq \alpha \leq 6\,\text{deg}$. They observed that increasing the APG caused the reattachment length to increase, whereas it decreased in a FPG. Ra and Chang [16] investigated separated and reattached flow downstream of a backward-facing step. They investigated several curvatures of the top wall to create the pressure gradient immediately downstream of the step and reported the pressure-coefficient distribution and the reattachment length. They found that the reattachment length increased with an increase in pressure gradient. Driver and Seegmiller [13] studied separated and reattached flows in diverging channels behind a backward-facing step using LDA. A deflected top wall at an angle $\alpha = 6\,\text{deg}$ was used to create the pressure gradient immediately downstream of the step. Detailed measurements of the mean velocity and turbulent quantities were reported as far downstream as 32 step heights. The reattachment length was found to increase under the influence of an APG. They observed that the turbulent kinetic energy and Reynolds shear stress tend to diffuse and convect farther from the lower wall in the diverging channel. Furthermore, the triple correlations diminished rapidly on the lower wall upon approaching reattachment and the production of turbulent kinetic energy decreased in the case of an adverse pressure gradient downstream of the step.

Although detailed experimental as well as direct numerical simulation and large eddy simulation studies (Le et al. [17]) of separated flows in ZPG and CC have been reported, separated and reattached flows in the presence of pressure gradients lack comprehensive studies. Furthermore, the effects of pressure gradients on separated and reattached flows, especially in the separated region, are relatively less understood. This paper reports new benchmark data sets in turbulent flow downstream of a two-dimensional rib in adverse and favorable pressure gradients. The favorable and adverse pressure gradients were produced in an asymmetric converging and diverging channels, respectively, that were preceded and followed by parallel sections. A PIV technique was used to conduct the velocity measurements, and profiles of mean velocities, turbulent intensities, Reynolds shear stress, and higher-order moments are reported in the separated and redevelopment regions as far downstream as 200 step heights. The insight provided by this study into adverse and favorable pressure gradients and the benchmark data sets reported will be valuable for validating complex near-wall turbulence models. The channels used in the present study have been employed in the past to study the effect of pressure gradients on turbulent flows with no ribs attached to the channel floor (Shah and Tachie [18]) and also over arrays of transverse ribs (Tachie [19]). Selected data from the study (obtained in the absence of the ribs) at an identical approach velocity will be compared with the presented results.

II. Experimental Setup and Measurement Procedure

A. Test Sections

The experiments were performed in a parallel-walled channel, an asymmetric diverging channel, and an asymmetric converging channel, hereafter referred to as tests CC, APG, and FPG, respectively. These channels were inserted into an existing water channel with a test section that is 2500 mm long, 200 mm wide, and 200 mm deep. As shown in Fig. 2a, the CC channel is 2500 mm long and has a half-channel height $h = 34.5$ mm. For the APG and FPG channels (Figs. 2b and 2c), the first 1000-mm (OA) and the last 500-mm (BC) sections have straight parallel walls, whereas the 1000-mm section (AB) located between these parallel sections diverges nonlinearly from a height of 54 to 84 mm for the APG case and converges from 84 to 54 mm for the FPG case. The zero location for the x coordinate ($x = 0$) is taken at 1000 mm from the inlet of the test section, which also marks the start of convergence/divergence (A), $y = 0$ on the lower wall, and $z = 0$ at the midplane of the channel. The heights of the variable channels for APG and FPG are, respectively, given by

$$2h(x) = 54 - 7.39 \times 10^{-4}x + 5.73 \times 10^{-5}x^2 - 3.12 \times 10^{-9}x^3 - 5.09 \times 10^{-11}x^4 + 2.78 \times 10^{-14}x^5 \quad \text{(1a)}$$

$$2h(x) = 84 - 4.01 \times 10^{-2}x + 2.09 \times 10^{-5}x^2 - 7.17 \times 10^{-8}x^3 + 8.83 \times 10^{-11}x^4 - 2.78 \times 10^{-14}x^5 \quad \text{(1b)}$$

where x is measured in millimeters and the relationship is valid in the range of $0 \leq x \leq 1000$. As mentioned earlier, these channels have been used previously by Shah and Tachie [18] (with no obstacles attached on the channel floor) to investigate the effects of APG and FPG on the mean flow and turbulent statistics. As explained in that study, the choice of the preceding channel distribution $h(x)$ was

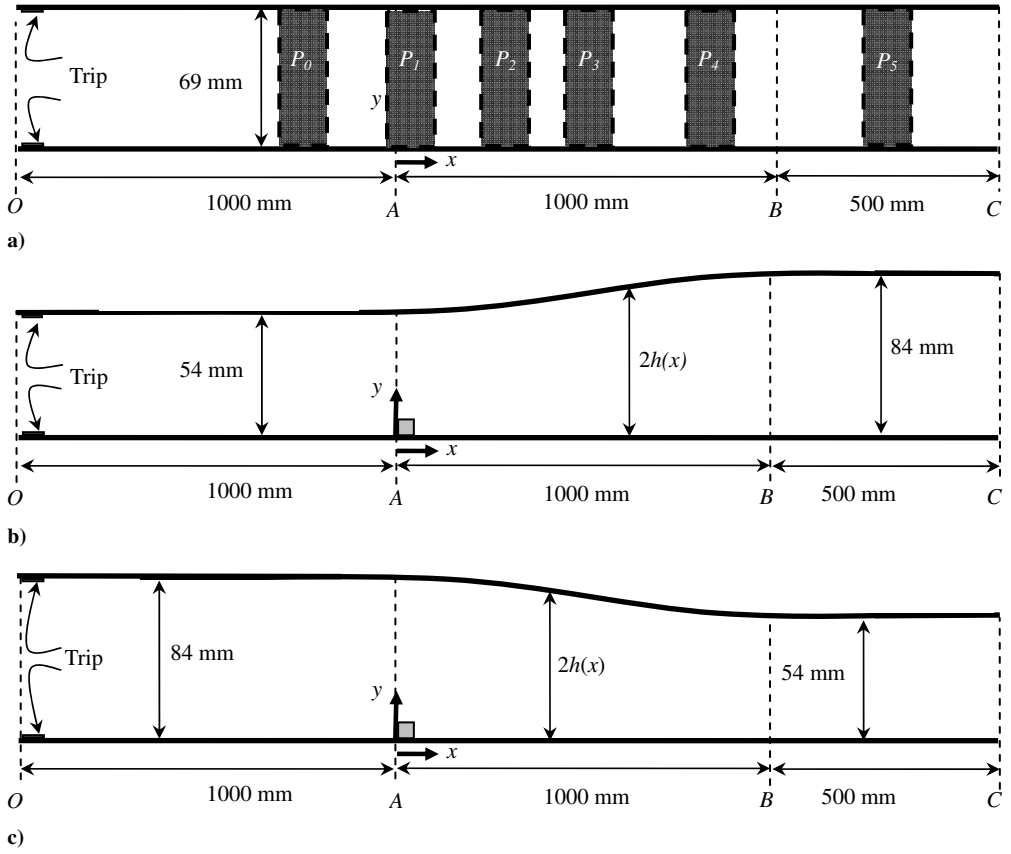

Fig. 2 Experimental setup: a) parallel-walled channel, b) diverging channel, and c) converging channel; dashed regions P_0 to P_5 denote x–y planes in which PIV measurements were made for a channel (not to scale).

partly constrained by the test section of the existing main water channel and the need to obtain two-dimensional mean flow at the midplane of the converging and diverging channels. A number of distributions were tried, and the pressure gradient along the channel was analytically calculated assuming inviscid flow. The preceding distributions were chosen because they produced pressure gradients that were not too severe to cause flow separation in the APG channel or relaminarization in the FPG channel, yet high enough to noticeably modify the flowfield compared with that in a channel with parallel walls.

B. PIV System and the Measurement Procedure

The flow was seeded with 5-μm polyamide seeding particles with a specific gravity of approximately 1.03. An Nd-YAG laser (120 mJ/pulse) of 532-nm wavelength was employed to illuminate the flowfield. The laser sheet was located at the midplane of the channel. A 12-bit HiSense 4M camera (2048 × 2048 pixel CCD array size and a 7.4-μm pixel pitch) was coupled to a 60-mm AF Micro Nikkor lens. The instantaneous digital images were postprocessed by the adaptive-correlation option of the commercial software developed by Dantec Dynamics (FlowManager 4.50.17). The adaptive correlation uses a multipass fast Fourier transform cross-correlation algorithm to determine the average particle displacement within the interrogation area. A three-point Gaussian curve fit was used to determine particle image displacement with subpixel accuracy. The particle image diameter was estimated to be $d_p = 16.8$ mm (2.27 pixels), 16.7 μm (2.26 pixels), and 16.7 μm (2.23 pixels) in tests CC, APG, and FPG, respectively. These values are in good agreement with a value of 2.0 recommended by Raffel et al. [20] to minimize peak locking. A sample size of 2040 images and an interrogation area of 32 × 16 pixels with 50% overlap were used to compute the mean velocity and turbulent statistics reported subsequently. The choice of 2040 images and 32 × 16 pixels with 50% overlap were based on comprehensive convergence and spatial resolution tests conducted using typical profiles of the mean velocity, turbulent intensities, Reynolds shear stress, and triple correlations in the separated region ($x/k = 4$) and the redevelopment region ($x/k = 21$). These results are presented by Shah and Tachie [6]. Based on the friction velocity for the approach boundary layer, the spatial resolution in wall variables was, respectively, $\Delta y^+ = 7.9$, 9.0, and 8.3 in tests CC, APG, and FPG. According to the recent study conducted by Shah et al. [21], these values are adequate to resolve the inner region of smooth- and rough-wall turbulent flows.

There are many sources of measurement uncertainty in PIV measurements. The guidelines and steps necessary to minimize these errors are discussed by Prasad et al. [22] and Forliti et al. [23]. Following the methodologies proposed and explained by Coleman and Steele [24], the uncertainty in the mean velocities at a 95%-confidence level was determined to be ±2%. The uncertainties in turbulent intensities and Reynolds shear stress were estimated to be ±5 and ±10%, respectively; ±15% for the third-order moments. In the graphs shown subsequently, error bars are used to indicate the measurement uncertainties at a 95%-confidence level.

C. Test Conditions

A 75-mm-wide strip made of four 3-mm-wide rectangular bars, 21 mm apart, was used on the upper and lower walls of the channel entrance to ensure a rapid development of the turbulent boundary layer. The two-dimensional square rib of height $k = 6$ mm was glued to the bottom of the channel at $x = 0$ (1000 mm from the inlet of a given channel) to cause flow separation for the three cases. For the APG channel, additional measurements were made, with the ribs placed at an upstream section of the diverging section ($x/k = -25$) and within the diverging section ($x/k = 0$ and 25). The goal was to study how rib location, relative to the inlet section of divergence, modifies the flowfield. Because no significant effects of rib location on the flow characteristics were observed, only data obtained at $x = 0$ for the APG channel will be discussed in detail in subsequent

Table 1 Summary of upstream flow parameters

Test	U_o, m/s	δ, mm	δ^*, mm	θ, mm	H	Re_k	Re_θ	k/δ	$k/2h$	$k^+ = kU_\tau/\nu$
CC	0.445	19	2.2	1.4	1.57	2640	620	0.31	0.09	140
APG	0.460	21	2.8	1.8	1.55	2760	830	0.29	0.11	140
FPG	0.464	39	3.6	2.5	1.44	2760	1150	0.15	0.07	140

sections. For each test condition (i.e., tests CC, APG, and FPG), reference measurements were made in an x–y plane upstream of the rib (denoted as P_0 in Fig. 2a) to characterize the approach flow and then in five planes (P_1–P_5) located around and downstream of the rib. From these measurement planes, profiles were extracted at $x/k = -30, 1, 2, 4, 9, 13, 21, 30, 50, 120$, and 200. It should be noted that the location $x/k = 200$ is within the downstream parallel section (AB). A summary of some of the upstream parameters is presented in Table 1. For a given test condition, U_o is the maximum streamwise velocity, δ is the boundary-layer thickness defined as the y location at which the local velocity is 99% of U_o, δ^* is the displacement thickness, θ is the momentum thickness, Re_k is the Reynolds number based on U_o and k, Re_θ is Reynolds number based on U_o and θ, and k/δ is the perturbation strength. The boundary-layer thickness, as well as the displacement and momentum thicknesses, of the approach flow is nearly the same in test CC and test APG. The shape parameter obtained for the three test cases are similar and compare reasonably well with prior data at similar Re_θ (Purtell et al. [25]). The perturbation strength k/δ of 0.31, 0.29, and 0.15, respectively, in tests CC, APG, and FPG implies a weak perturbation according to the classification proposed by Bradshaw and Wong [1]. The blockage ratio $k/(2h)$, where $2h$ is the channel height at $x = 0$, and the ratio of the rib height to the viscous length scale of the approach flow ($k^+ = kU_\tau/\nu$, where U_τ is the friction velocity) are also summarized in Table 1. It should be noted that the crest of the rib is well within the logarithmic layer in all the tests. Because $k^+ = 140$ in tests CC, APG, and FPG, it implies that the distortion of the inner layer of the approach boundary layer by the rib is identical in all the tests.

III. Results and Discussion

A. Isocontours of Mean and Turbulent Quantities

The isocontours of the mean velocity U, mean spanwise vorticity $\Omega_z = \partial V/\partial x - \partial U/\partial y$, and Reynolds shear stress $\langle -uv \rangle$ were obtained to reveal some qualitative features of the flow pattern in the vicinity and downstream of the rib (Fig. 3). The data are made dimensionless using the approach velocity U_o and rib height k. The corresponding mean streamlines are superimposed on each plot to show the extent of the recirculation region and to relate the turbulent quantities to the mean flow pattern. The vertical axis is shown up to $y = 6k$, which is above the half-channel height in test APG ($h = 4.5k$), near the half-channel height of test CC ($h = 5.75k$), and below that of test FPG ($h = 7k$). In each case, the flow separates close to the leading edge of the rib and is deflected upward from the rib. As expected, a recirculation bubble is formed downstream of the rib and the flow subsequently reattaches. A counterclockwise rotating vortex at the downstream edge of the rib can also be observed. The lower half of the recirculation bubble is dominated by reverse flow with a maximum magnitude of $0.2U_e$ located at $x/k \approx 4$ to 5 and adjacent to the floor. The reattachment length x_r was estimated as the x location at which the separated streamline reattached on the floor. It was found that $x_r/k = 10.4$, 10.3, and 9.8, respectively, in tests CC, APG, and FPG. The x_r/k values in tests CC and APG are almost identical, whereas the value for FPG is only 5% smaller. The reattachment length is a sensitive parameter that depends on various parameters. For example, it increases with increasing k/δ (Eaton and Johnston [26]) and is negatively correlated with freestream turbulence (Castro [27]). Castro [27] reported a value of x_r that ranged from $x_r/k = 9$ to 11 for a boundary-layer thickness of 0.069 to $0.169k$. The closeness of x_r/k values in the present study may be partly due to the notion that the inner layer of the approach boundary layer was equally distorted in all the tests. Furthermore, the distributions of the maximum velocity and the acceleration/deceleration parameter in the separated region ($0 < x/k < 12$) do not vary significantly from test to test (Figs. 4a and 4b). The present value of $x_r/k = 10.4$ for test CC ($k/d = 0.31$) is 10% lower than the $x_r/k = 11.5$ reported by Bergeles and Athanassiadis [9], but in that study, the blockage ratio was higher ($k/\delta = 0.48$) and the background freestream turbulence was lower (0.5%, compared with background turbulence of 5% in the present study). Both effects (higher k/δ and lower turbulence level) would increase the reattachment length. Agelinchaab and Tachie [28] reported a value of $x_r/k = 8.5$ in their open-channel flow over a square rib ($k/\delta = 0.11$).

The mean flow patterns are similar for the three cases, but the rib affects a greater portion of the channel height in test APG than in test FPG. The isocontours of the mean spanwise vorticity reveal regions of intense shear layer close to the rib. Because $\partial V/\partial x \ll \partial U/\partial y$, values of Ω_z are negative everywhere except in the very-near-wall region inside the separation bubble. The bulk vorticity is generated at the top plane of the rib and convected downstream. The Reynolds shear stress also reveals regions of high turbulence levels in the vicinity of the separated shear layer.

B. Boundary-Layer Parameters

The boundary-layer parameters (Fig. 4) can provide insight into the characteristics of boundary-layer separation and its subsequent redevelopment. Because of the asymmetric nature of the flow, these parameters were evaluated in both the lower and upper boundary layers, which are defined, respectively, as the flow region from the lower wall up to the location of U_e, and from the upper wall to the location of U_e. The values of U_e/U_o at selected x locations within the various planes of measurement are plotted in Fig. 4a. Except for the plane containing the rib, P_1, a linear variation of U_e with x was assumed and $\mathrm{d}U_e/\mathrm{d}x$ was evaluated as the slope of a least-squares linear fit to U_e versus x. Because U_e varied nonlinearly with x within the separated region P_1, a fifth-order polynomial was fitted to the measured data and the curve fit was differentiated to estimate $\mathrm{d}U_e/\mathrm{d}x$. The values of the dimensionless acceleration/deceleration parameter $K = (\nu/U_e^2)(\mathrm{d}U_e/\mathrm{d}x)$ are plotted in Fig. 4b. In the upstream parallel section (not shown), the acceleration parameter was $K = 0.13 \times 10^{-6}$. For comparison, selected data obtained in the same channels (but with no ribs) and at identical $U_o(0.460 \pm 0.001$ m/s) are shown. The previous data show the expected trend within the variable section and downstream parallel section of the channel. For example, U_e increased consistently in the APG and decreased in the FPG. Furthermore, K is negative and positive, respectively, in the APG and FPG in the variable section and becomes nearly zero at the downstream parallel section of each channel. Regardless of the pressure gradient, it is evident that the blockage produced by the rib caused the flow to accelerate up to $x/k = 4$ (which approximately corresponds to the center of the recirculation bubble), followed by a region of flow deceleration down to $x/k = 13$. In this region, the magnitude of K in test FPG is only 50% of the values obtained in test CC and test APG. Beyond the reattachment location, the velocity variation remains nearly constant in test CC, whereas it decreases monotonically in test APG and increases in test FPG. At $x/k = 120$, for example, U_e is only 3% different from its upstream value in test CC, but it is 40% higher in test FPG and 20% lower in test APG. The pressure-gradient distortion caused by the rib seems to disappear ($K \approx 0$) beyond $x/k = 20$ in test CC, but the combined effects of the rib and the pressure gradients persists up to $x/k = 120$ in tests APG and FPG. It

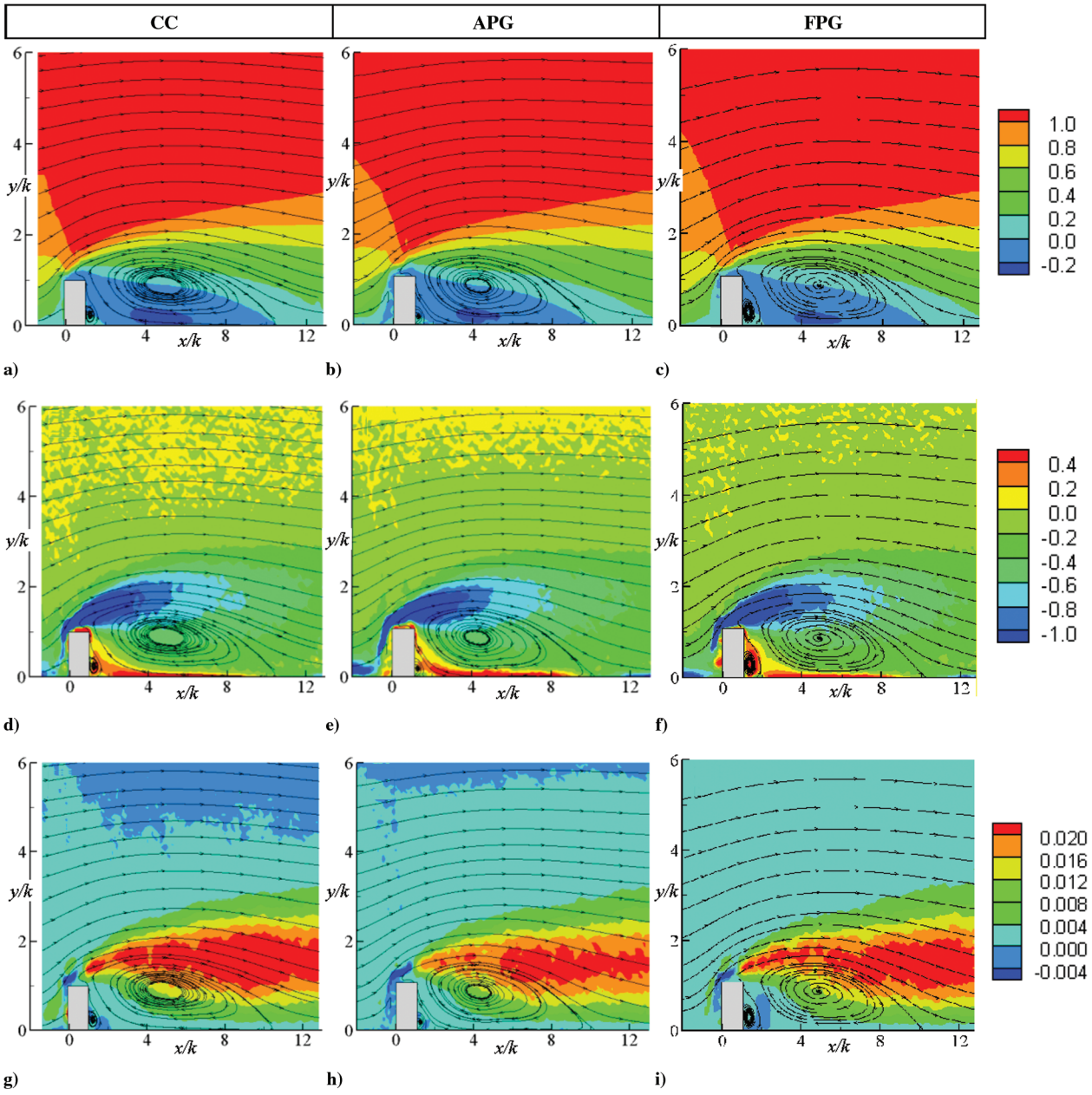

Fig. 3 Isocontours of mean and turbulent quantities: a–c) U, d–f) Ω_z, and g–i) $-uv$.

is important to note that the values of U_e and K with or without a square rib attached to the channel floor for a particular pressure gradient (e.g., FPG) are not significantly different in the region $x/k > 30$. This would imply that the pressure gradient has stronger effects on the mean flow at these locations than the distortion produced by the ribs.

The values of δ, $y_{\max}$ (wall normal distance from the lower wall to the location of local U_e), δ^*, and θ normalized by the local half-channel height are plotted in Figs. 4c–4h. In the absence of the ribs, the APG thickened the boundary-layer parameters (and vice versa for the FPG). The boundary-layer thickness and $y_{\max}$ obtained in the present study exhibit a nearly linear growth up to $x/k < 120$. On the other hand, δ_L^* and θ_L increase to a maximum value at $x/k = 7$ and 21 (except θ in test APG, which is at $x/k = 30$) and then begin to decrease monotonically. Even with the rib attached to the floor, as in the present study, the APG thickened the lower boundary layer and produced significantly larger values of δ_L/h, δ_L^*/h, and θ_L/h than in test CC. On the other hand, the values obtained in test FPG are either smaller than or similar to those obtained in test CC. The trends observed for δ_L^* and θ_L are similar to those reported by Driver and Seegmiller [13] for their wall divergence of $\alpha = 0$ and 6 deg. Although the values of δ_U^*/h and θ_U/h vary from one test to the other, these differences are significantly smaller than in the lower boundary layer.

C. Flow Development Downstream of the Rib

In this section, profiles of the mean velocities, turbulent quantities, and terms in the transport equation for turbulent kinetic energy at selected streamwise locations in the separated region ($x/k = 1, 2, 4, 9$) and the redevelopment region ($x/k = 13, 21, 30, 50, 120, 200$) in tests CC, APG, and FPG are plotted together to document the effects of the pressure gradient on the flow development downstream of a rib. For comparison, the upstream profile is also plotted at each x/k location. Typical profiles obtained in the variable sections of the FPG channel (at $x/k = 123$) and APG channel (at $x/k = 140$) from Shah and Tachie [18] are compared with those obtained in the present study at $x/k = 120$. Similarly, profiles that were obtained at $x/k = 224$ in the FPG channel and at $x/k = 205$ in the APG channel in the previous study are compared with those obtained at $x/k = 200$ in the present study. Although the x/k locations are not identical in the previous and present studies, the comparison is still invaluable. The

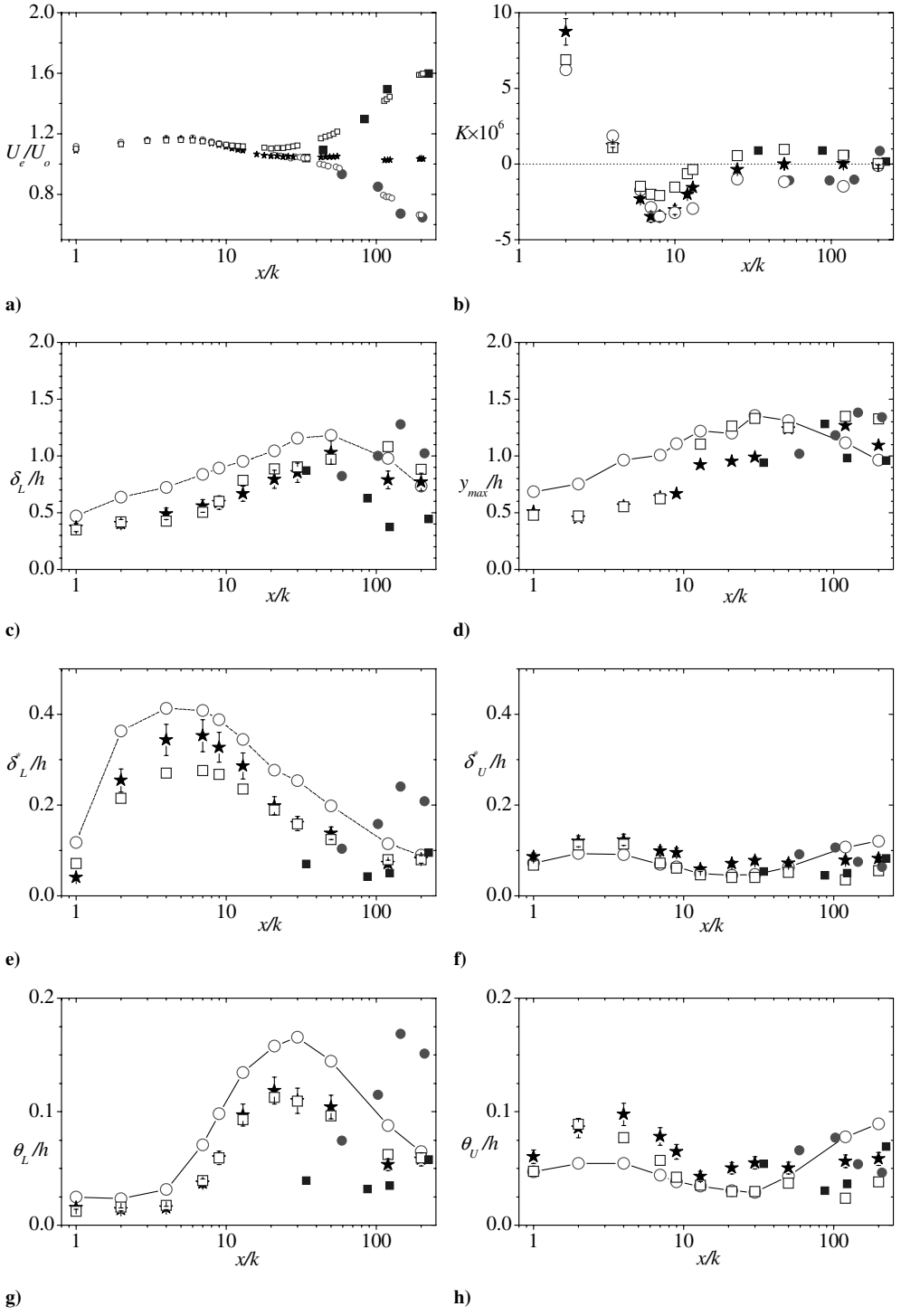

Fig. 4 Boundary-layer parameters: a) U_e/U_o, b) K, c) δ_L/h, d) $y_{\max}/h$, e) δ^*_L/h, f) δ^*_U/h, g) θ_L/h, and h) θ_U/h; CC ★, APG ○, and FPG □; reference APG ● and FPG ■ data are from Shah and Tachie [18].

local maximum velocity U_e and half-channel height h are used as the appropriate velocity and length scales.

1. Mean Velocity Profiles

The mean streamwise velocity profiles, shown in Figs. 5a and 5b, reveal only marginal effects of the rib and pressure gradient on the upper boundary layer, except at $x/k = 120$ and 200, for which the present profiles in test APG is less full than the others. This would imply that any effects resulting from the differences in blockage ratio in the various tests should be confined to the lower boundary layer. As expected, the presence of the rib considerably reduced the values of U close to the lower wall. Consequently, the lower-boundary-layer profiles downstream of the rib become less full, compared with the reference upstream profile. The maximum backflow is approximately $0.2U_e$ for all the test cases, a value that is similar to those reported in previous studies (Tachie et al. [29] and Eaton and Johnston [26]). The profiles obtained in the APG are the most distorted and the variation of U with y from the lower wall is also more gradual in test APG than in the other profiles. The implications of this observation to turbulence production will be discussed later. The mean velocity recovered back toward the upstream profile at $x/k = 200$ and, as expected, the recovery process is slowest in test APG. The profiles obtained at $x/k = 120$ and 200 in the FPG (with or without ribs) are nearly indistinguishable. In test APG, on the other hand, the present profiles are in better agreement with the reference upstream profile than if no rib was attached to the floor.

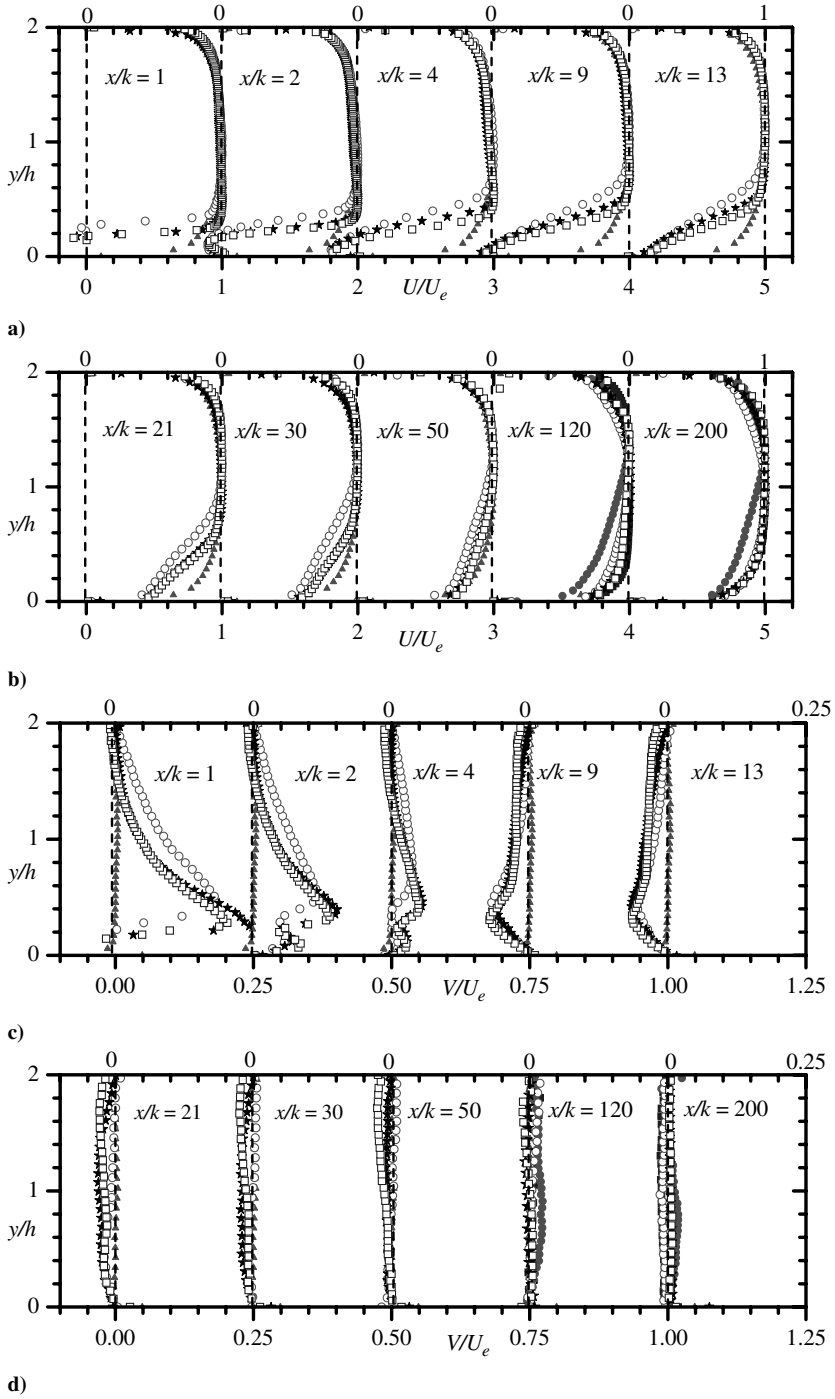

Fig. 5 Mean velocity profiles at various streamwise locations: a–b) mean streamwise velocity, and c–d) mean transverse velocity; upstream ▲, CC ★, APG ○, and FPG □; reference APG ● at $x/k = 140$ and 205 and FPG ■ profiles at $x/k = 123$ and 224 are from Shah and Tachie [18].

The mean transverse velocity V is nearly zero upstream of the rib, but at $x/k = 1$, its value increased to 0.2 to $0.25U_e$ (Figs. 5c and 5d). The values of V are predominantly positive in the region $x/k \leq 4$ because, as shown in Fig. 3, the mean streamlines curve upward as the rib is approached. Beyond $x/k = 4$, the streamlines curve downward, resulting in negative velocity. The transverse velocity decays rapidly downstream of the recirculation. At $x/k = 21$ and 200, for example, the values of V/U_e are, respectively, less than 4 and 1% for all test cases.

2. *Turbulent Intensities and Reynolds Stress*

The streamwise and transverse turbulent intensities are plotted in Fig. 6. In the separated region and the early stage of flow redevelopment ($x/k \leq 50$), the values of $u'_{\min}/U_e$ and $v'_{\min}/U_e$ are nearly independent of pressure gradient. In this region, the distributions of the turbulence intensities in the outer boundary layer are also only marginally affected by pressure gradient. Although the background turbulence level in the present study (e.g., $u'_{\min}/U_e \approx 0.05$) is an order of magnitude higher than typical values reported in wind-tunnel experiments, they are comparable with data reported in other two-dimensional channel flows. For example, Durst et al. [30] compiled $u'_{\min}/U_e$ values reported in 16 different experiments and concluded that $u'_{\min}/U_e = 0.04 \pm 10\%$. Irrespective of the pressure gradient, the turbulence level rises consistently until $x/k = 9$ (which is approximately one step height upstream of the reattachment point) and then begins to decay rapidly beyond $x/k = 13$. At $x/k = 9$, the peak values of the turbulent intensities in

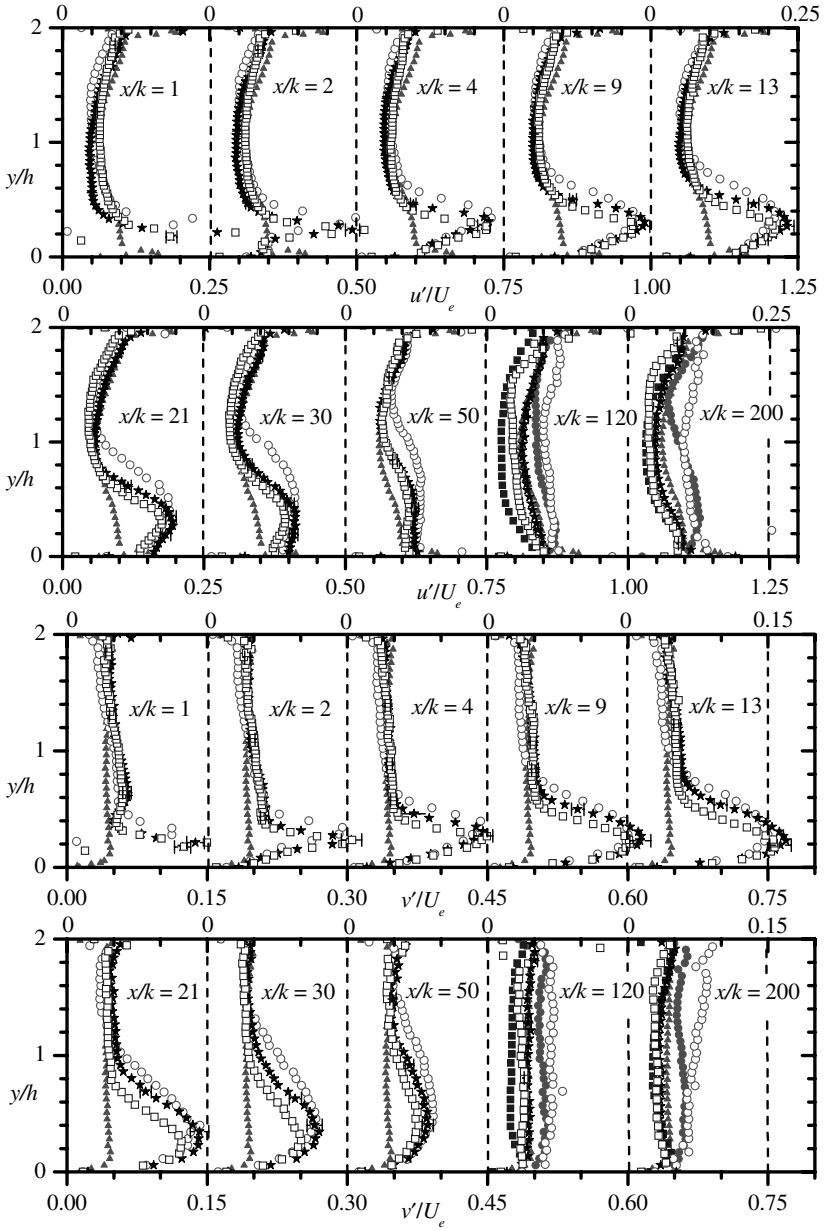

Fig. 6 Turbulence intensity profiles at various streamwise locations: a–b) streamwise turbulence intensity and c–d) transverse turbulence intensity; upstream ▲, CC ★, APG ○, and FPG □; reference APG ● at $x/k = 140$ and 205 and FPG ■ profiles at $x/k = 123$ and 224 are from Shah and Tachie [18].

test APG, test FPG, and test CC are $(u'/U_e)_{\max} = 0.23 \pm 0.01$ and $(v'/U_e)_{\max} = 0.15 \pm 0.01$, which are approximately 40% higher than the corresponding upstream values. The region of enhanced turbulence levels coincides with the flow region of strong shear layer in Fig. 5. As the flow evolves downstream of the rib and the shear layer propagates outward from the lower wall, so does the region of high turbulence levels. Similar to the mean flow, the region of elevated turbulence level represents a larger fraction of the local channel height in test APG than in test FPG and test CC. At $x/k \geq 120$, all the profiles regain their symmetry with respect to the channel midplane. In this region, the profiles in test CC collapsed reasonably well with the corresponding upstream profile. On the other hand, profiles obtained in the FPG are lower than the upstream profiles, whereas those obtained in the APG are still higher than the upstream profiles. These observations are valid for the present and previous data.

The Reynolds shear stress (Figs. 7a and 7b) exhibits a similar trend as the turbulence intensities. In these cases, the peak values of $(\langle -uv \rangle / U_e^2)_{\max}$ at $x/k = 9$ are about 10 times as high as the upstream value. In accordance with the shear layer, the Reynolds shear stress is negative in the recirculation region adjacent to the lower wall.

Figure 8 shows the y locations at which $-uv$ changes sign ($y_{uv=0}$) and also at which the maximum values of U (y_{Ue}), u ($y_{u',\max}$), v ($y_{v',\max}$), $-uv$, and ($y_{\langle -uv \rangle,\max}$) occurred at selected streamwise locations in the region $0 \leq x/k \leq 30$. The dividing streamline, which separates the core flow from the main recirculating flow, is also plotted for the FPG. The y_{Ue} location increases monotonically with x (Fig. 8a). However, the increase is more dramatic in the separated region and in the vicinity of reattachment ($x/k \leq 12$) than downstream in the redevelopment region ($x/k \geq 20$). According to the eddy viscosity models, $\langle -uv \rangle = \nu_t \partial U/\partial y$, and hence $y_{Ue} \approx y_{\langle uv \rangle = 0}$. This condition is met downstream of reattachment, but in the separated region, y_{Ue} is closer to the wall than is $y_{uv=0}$. Along the first half of the separation bubble, $u'_{\max}$, $v'_{\max}$, and $\langle -uv_{\max} \rangle$ occur approximately along the dividing streamline (Figs. 8b–8d). However, near the reattachment location and beyond, the locations of the maximum values depart from the dividing streamline and move further away from the wall. Ruderich and Fernholz [4] also reported

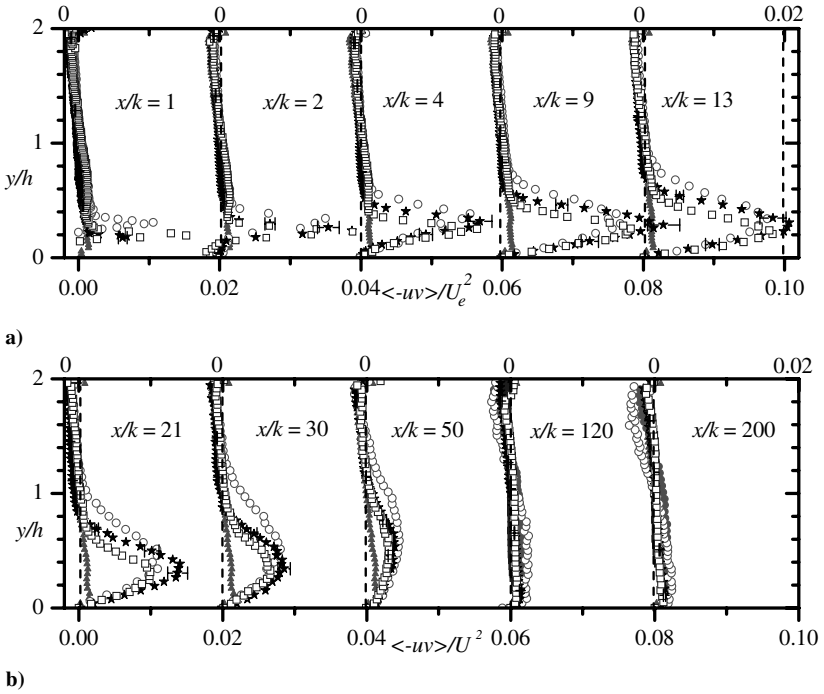

Fig. 7 Reynolds shear stress profiles at various streamwise locations; upstream ▲, CC ★, APG ○, and FPG □; reference APG ● at $x/k = 140$ and 205 and FPG (■) profiles at $x/k = 123$ and 224 are from Shah and Tachie [18].

that $y_{u',\max}$, $y_{v',\max}$, and $y_{\{-uv\},\max}$ fall on the dividing streamline in the range of $0 \leq x/x_r \leq 0.5$. In general, these values are higher in test APG than in tests CC and FPG downstream of the reattachment.

The distribution of the stress ratios (Fig. 9) provides insight into large-scale anisotropy. Because standard two-equation turbulence models (e.g., k-ε and k-ω) implicitly assume local isotropy, the information presented herein will be invaluable to turbulence modelers. Figures 9a and 9b show that the degree of anisotropy is certainly higher close to the upper wall, irrespective of the pressure gradient and the flow regions. The inherent intense mixing within the separated region promotes isotropy (i.e., $\langle v^2 \rangle / \langle u^2 \rangle$ is closer to unity), particularly in the vicinity of the lower wall, compared with the upstream profile. This observation also implies that the mechanism responsible for redistributing turbulent kinetic energy into $\langle u^2 \rangle$ and

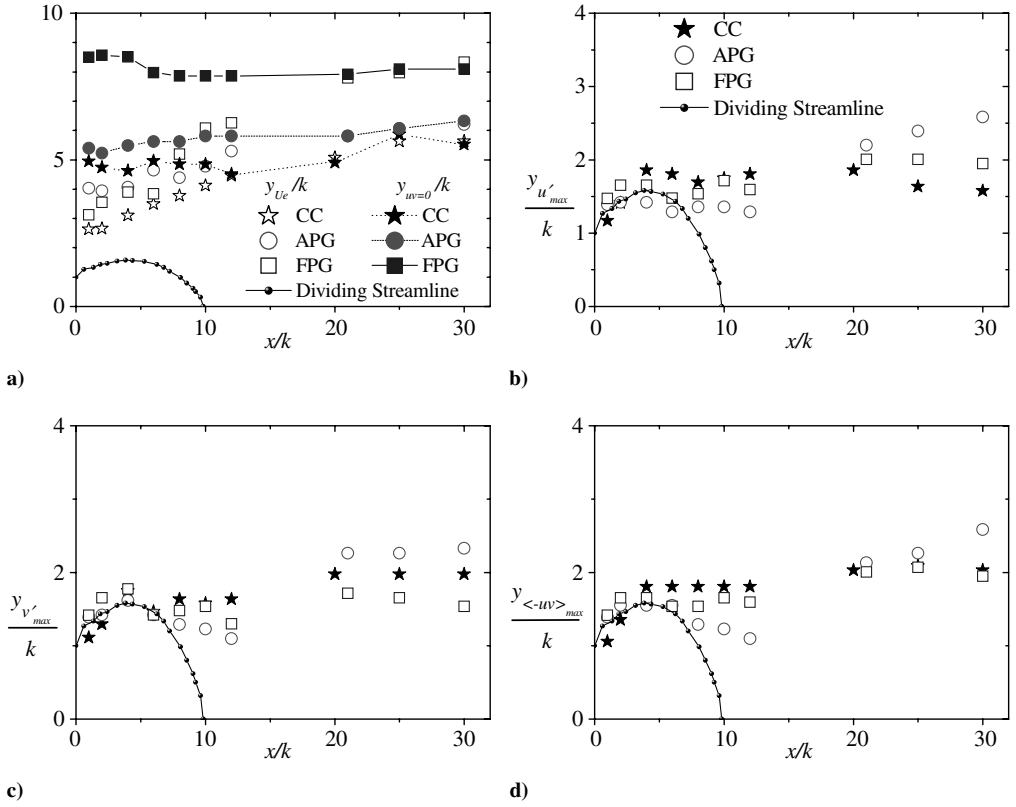

Fig. 8 The y locations corresponding to maximum mean and turbulent quantities at various streamwise locations: a) y_{Ue}, b) $y_{u',\max}$, c) $y_{v',\max}$, and d) $y_{\{-uv\},\max}$.

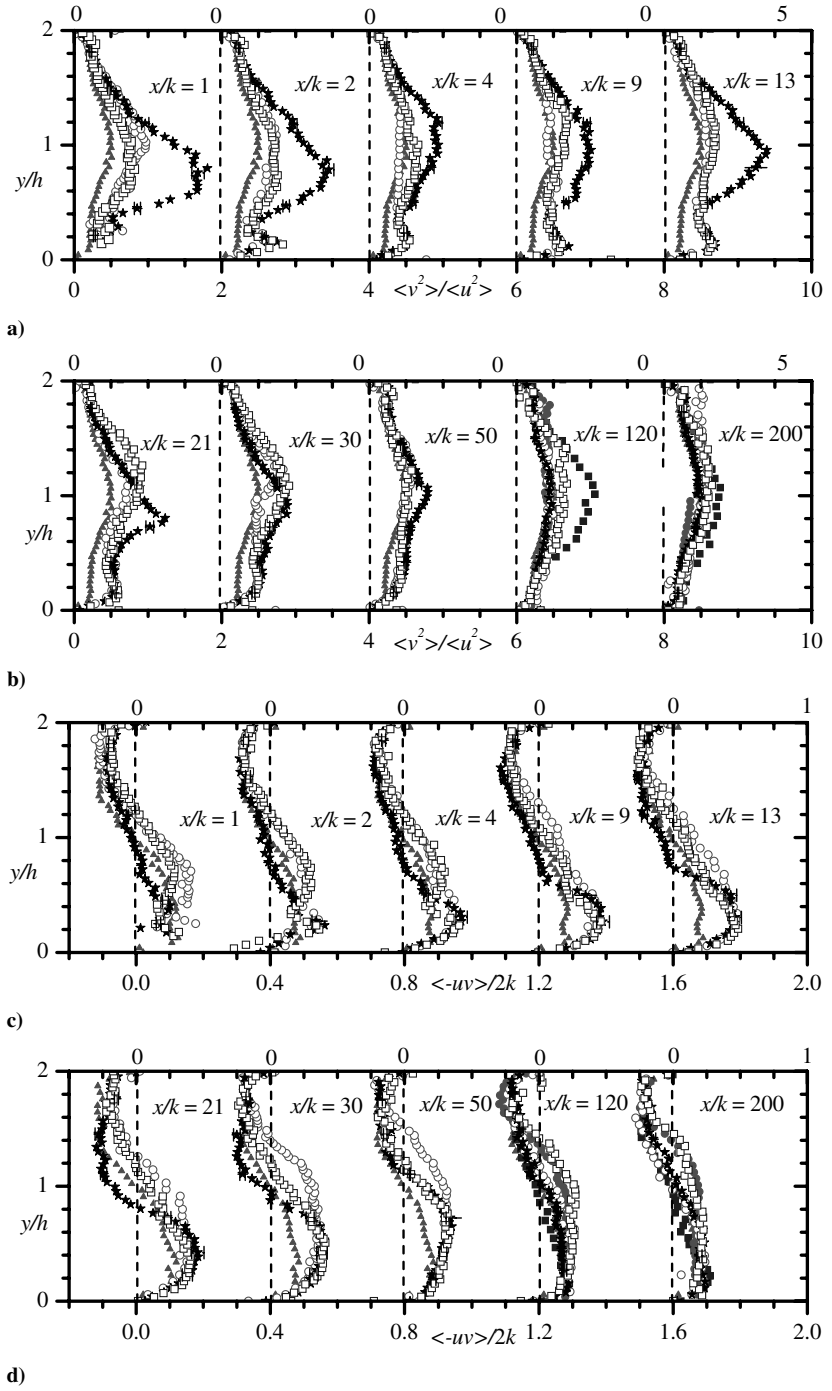

Fig. 9 Reynolds stress ratios at various streamwise locations: a–b) $\langle v^2\rangle/\langle u^2\rangle$ and c–d) $\langle -uv\rangle/2k$; upstream ▲, CC ★, APG ○, FPG □; reference APG ● at $x/k = 140$ and 205 and FPG ■ profiles at $x/k = 123$ and 224 are from Shah and Tachie [18].

$\langle v^2\rangle$ in separated flows and the canonical upstream flow is different. In general, turbulence models that cannot distinguish between the various Reynolds normal stresses would not be suitable for the flowfield investigated in this work. Downstream of reattachment, the profiles progressively return to the upstream profile. The FPG flow without the rib is the most isotropic. In their APG equilibrium boundary layers, however, Skåre and Krogstad [31] reported that the stress ratios are independent of pressure gradient.

Townsend's structure parameter $\langle -uv\rangle/2k$ is important for calibrating the turbulence model. In the present study, the turbulent kinetic energy was approximated from $k = 0.7[\langle v^2\rangle + \langle u^2\rangle]$. The structure parameter is typically taken as 0.15 in zero-pressure-gradient flows. For example, a value of $\langle -uv\rangle/2k = 0.15$ has been specified by Harsha and Lee [32], with 0.12 specified by Launder et al. [33]. The low values $|\langle -uv\rangle/2k|_{\max} \approx 0.1$ obtained upstream of the ribs may be partly due to low Reynolds number effects. Figures 9c and 9d show that $|\langle -uv\rangle/2k|$ is as high as 0.2 in the separated region and early stage of redevelopment ($4 \le x/k \le 21$) and reduces to 0.15 and 0.1, respectively, in the regions $30 \le x/k \le 50$ and $120 \le x/k \le 200$. The profiles are independent of the pressure gradient, except that the y/h locations at which $\langle -uv\rangle/2k$ changes sign are different for the various test conditions.

3. *Triple Correlations and Turbulent Kinetic Energy Budget*

The triple correlations are important turbulence statistics because their gradients constitute the turbulent diffusion terms in the transport equations for the turbulent kinetic energy and Reynolds stresses. For example, $\partial\langle uv^2\rangle/\partial y$ and $\partial[\langle u^2v > + \langle v^3\rangle]/\partial y$ are associated with the transport of $\langle uv\rangle$ and $\langle u^2\rangle + \langle v^2\rangle$, respectively, in the transverse

direction. The following four quantities were obtained and reported by Shah and Tachie [6]: $\langle u^3 \rangle$, $\langle u^2 v \rangle$, $\langle u v^2 \rangle$, and $\langle v^3 \rangle$. Because of space limitation, however, only $\langle u^2 v \rangle + \langle v^3 \rangle$ is plotted in the present study (Fig. 10a). The levels of $\langle u^2 v \rangle + \langle v^3 \rangle$ are significantly enhanced downstream of the rib. The profiles exhibit the characteristic features of a free shear flow in the early stage of separation. For example, they are nearly antisymmetric about the centerline of the shear layer, reaching peak values to either side of the centerline of the shear layer, and tapering off to zero at the edge of the shear layer. The negative lobes of the $\langle u^2 v \rangle + \langle v^3 \rangle$ close to the lower wall have disappeared in the region of $x/k > 30$. Chandrsuda and Bradshaw [34] and Jović [35] also reported that the triple correlations on the wall side of the shear layer diminish rapidly upon approaching reattachment because the main contribution of the triple correlations comes from the large eddies that are rapidly attenuated close to the wall near reattachment. The levels of $\langle u^2 v \rangle + \langle v^3 \rangle$ have significantly reduced at $x/k = 50$, implying that their contribution of the turbulent transport (diffusion term) is diminished. Although the magnitude of the profiles is independent of the pressure gradient, it is evident that the region of nonnegligible diffusion represents a larger and a smaller fraction, respectively, of the diverging and converging channel heights, compared with the parallel-wall channel.

For a two-dimensional flow, the production P_k, dissipation ε_k, and convection C_k terms in the transport equation for the turbulent kinetic energy are as follows:

$$P_k = -[\langle uv \rangle (\partial U/\partial y + \partial V/\partial x) + (\langle u^2 \rangle \partial U/\partial x + \langle v^2 \rangle \partial V/\partial y)] \tag{2}$$

$$\varepsilon_k = \nu[2\overline{(\partial u'/\partial y)(\partial v'/\partial x)} + \overline{(\partial u'/\partial y)^2} + \overline{(\partial v'/\partial x)^2} + 2\overline{(\partial u'/\partial x)^2} + \overline{(\partial v'/\partial y)^2} + 2\overline{(\partial w'/\partial z)^2}] \tag{3}$$

$$C_k = 0.5[U(\partial \langle u^2 \rangle/\partial x + \partial \langle v^2 \rangle/\partial x) + V(\partial \langle u^2 \rangle/\partial y + \partial \langle v^2 \rangle/\partial y)] \tag{4}$$

The diffusion term for the turbulent kinetic energy was also evaluated, but those data are not shown because they showed scatter.

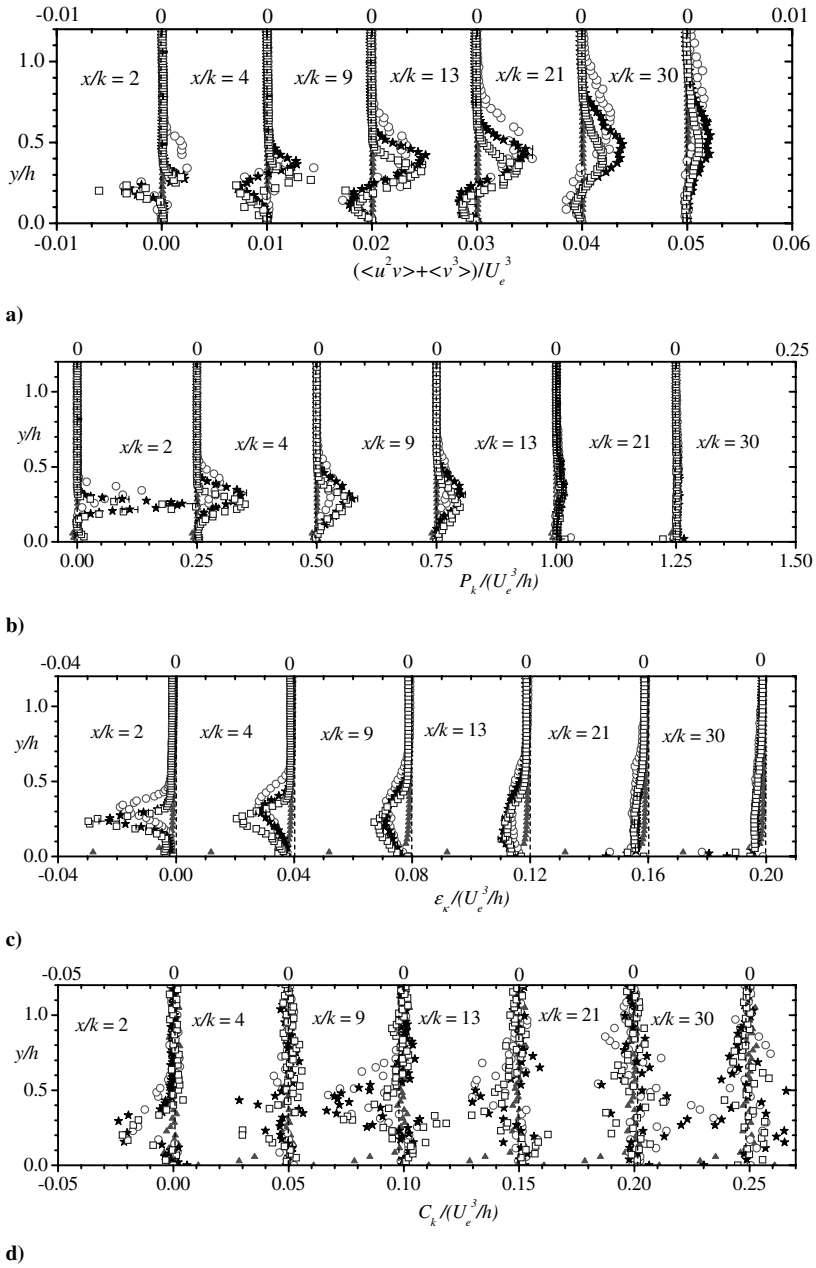

Fig. 10 Triple correlations and various terms for the Reynolds shear stress and turbulent kinetic energy budget at selected streamwise locations: a) $\langle u^2 v \rangle + \langle v^3 \rangle$, b) P_k, c) ε_k, and d) C_k; upstream ▲, CC ★, APG ○, and FPG □.

Because the spanwise velocity was not measured, the last term in the expression for Eq. (4) was estimated from the continuity equation for the fluctuating velocity components as follows:

$$\overline{(\partial w'/\partial z)^2} + \overline{(\partial u'/\partial x + \partial v'/\partial y)(\partial u'/\partial x + \partial v'/\partial y)} \quad (5)$$

Equation (5) is identical to that employed by Piirto et al. [8] in their PIV study of a backward-facing step. The gradient terms in the energy-budget equations were calculated using a second-order central-difference scheme. The budget terms at selected x locations in the separated region and in the redevelopment region are shown in Figs. 10b–10d. It was observed that $\partial U/\partial y \gg \partial V/\partial x$ everywhere, irrespective of the pressure gradient and streamwise location. Although, $\partial U/\partial x$ and $\partial V/\partial y$ are smaller than $\partial U/\partial y$, they are generally not negligible in separated region. The mean flow is approximately two-dimensional and $\partial U/\partial x \approx -\partial V/\partial y$ from continuity. The production of turbulent kinetic energy P_k consists of contribution from shear stresses (first two terms on the right-hand side) and normal stresses (last two terms). Because $\partial U/\partial y > \partial V/\partial x$ over most of the shear layer, $\langle -uv\rangle \partial U/\partial y$ is the dominant term for production by the shear stress. The magnitude of the production by the normal stresses ($\langle u^2\rangle \partial U/\partial x$ and $\langle v^2\rangle \partial V/\partial y$) is individually high; however, their sum is smaller than the individual terms. It should be noted that in Fig. 10b, the region of enhanced production levels coincides with the flow region of strong shear layer in the separated region. The production peak is lower in test APG than in tests CC and FPG, but the region of nonnegligible production is largest for test APG. This finding is similar to measured data obtained in the APG and FPG flows with no rib on the channel floor. It was observed from Figs. 5a and 5b that the variation of U with y is slowest (implying lower values of $\partial U/\partial y$) in test APG, whereas the peak values for the Reynolds shear and stresses are nearly similar for the three test conditions in the separated region. Because $\langle -uv\rangle \partial U/\partial y$ is the major contributor to the production terms, Fig. 10b is consistent with observations made in Figs. 5 and 7. The dissipation term (Fig. 10c) is substantially less than production so that the flow is not in the energy-equilibrium state. The imbalance $P_k \neq \varepsilon_k$ is due to nonnegligible transport of turbulent kinetic energy by the mean flow (convection) and turbulence diffusion (not shown), both of which are predominantly negative. Thus, Fig. 10 implies that turbulent models based on equilibrium assumptions would not be able to accurately predict flow in the recirculation region and in the early stage of flow redevelopment. At $x/k = 30$, the budget terms have significantly reduced. It is expected that as the flow evolves farther downstream, the diffusion and convection terms will eventually become negligible so that energy equilibrium will be established.

D. Lower Boundary Layer in the Redevelopment Region

In this section, the profiles of the mean velocity and Reynolds stresses obtained in the lower boundary layer of the redevelopment region are plotted using the friction velocity U_t. Although U_t is traditionally used to interpret the mean velocity profile, various studies conducted in pressure-gradient turbulent flows over smooth and rough surfaces showed that the mixed scaling $U_e\delta^*/\delta$ proposed by Zagarola and Smits [36] collapses the defect profiles better than U_τ. Therefore, the mean velocity defect profiles are also scaled using $U_e\delta^*/\delta$.

1. *Mean Velocity Profiles*

The log law has also been used in separated and reattached flows downstream of reattachment in previous studies. In the redevelopment region, Bradshaw and Wong [1] reported the presence of the log region for $(x - x_r)/k \geq 10$. In the present study, the friction velocity U_t was determined by fitting the measured mean velocity to the following law of the wall in the viscous sublayer [Eq. (6)], the classical log law [Eq. (7)], and the empirical formula [Eq. (8)] proposed by Spalding [37] to facilitate a smooth transition from the linear to the log region:

$$U^+ = y^+ \quad (6)$$

$$U^+ = \kappa^{-1}\,\ell_n\, y^+ + 5.0 \quad (7)$$

$$y^+ = U^+ + e^{5\kappa}(e\kappa^{U+} - 1 - \kappa U^+ - 0.5(\kappa U^+)^2 - 1/6(\kappa U^+)^3 - 1/24(\kappa U^+)^4) \quad (8)$$

where $U^+ = U/U_\tau$, $y^+ = yU_\tau/\nu$, $\kappa(=0.41)$ is the von Kármán constant, and ν is the kinematic viscosity.

Figures 11a–11c show the measured mean velocity profiles in the region $x/k \geq 13$, as well as in Eqs. (6–8). Equations (6) and (8) describe the measured data reasonably well in the region $y^+ < 30$. In most cases, data points were obtained in the linear viscous sublayer. No substantial logarithmic region exists at $x/k = 13$, and the profiles immediately downstream of the reattachment are characterized by a large wake component. The log-law region is limited to $y^+ \leq 150$ at $x/k = 21$ (Chandrsuda and Bradshaw [34]); however, as the streamwise distance increases, so does the extent of overlap region between the measured data and the log law.

The skin-friction values estimated from $C_f = 2(U_\tau/U_e)^2$, where U_τ is the friction velocity determined by fitting the measured mean velocity profiles to the log law, are plotted as an insert in Fig. 11b. Jović [10] and Le et al. [17] reported negative C_f values in the recirculation region and a value of $C_f = 0$ at the point of reattachment. Measurements of C_f in the recirculation region were not made, however, in the present study. The values of C_f rise rapidly from approximately 0.0006 at $x/k = 13$ to a value of about 0.005 at $x/k \geq 120$ (which is within 6% of the corresponding upstream value). The rapid rise of C_f downstream of reattachment is a common feature in the redevelopment region of separated and reattached flows (Ruderich and Fernholz [4] and Le et al. [17]). The previous results demonstrate that the variations of C_f exhibit discernible pressure-gradient effects. However, the values of C_f are nearly independent of pressure gradient in the presence of the rib. The C_f values were also estimated using the Ludweig–Tillman correlation:

$$C_f = 0.246 Re_\theta^{-0.268} 10^{-0.678H} \quad (9)$$

This correlation has been previously used in separated and reattached flows (Bradshaw and Wong [1]) and flows with pressure gradients (Cutler and Johnston [12]) to estimate C_f. The accuracy of the correlation depends on the values of δ^* and θ. The values of δ^* and θ are expected to be reliable because almost all data sets have measurements starting in the region $1 < y^+ \leq 10$. Note that in determining δ^* and θ, the measured data were extrapolated to the wall using $U = 0$ at $y = 0$. The differences between the C_f values obtained from the log law and Eq. (9) are within $\pm 10\%$.

The mean defect profiles normalized by U_τ are shown in Figs. 11d–11f and those normalized by the mixed scaling $U_e\delta^*/\delta$ are plotted in Figs. 11g–11i. The profiles in the region of $x/k < 120$ are distinctly different from the upstream profile. As the flow develops further downstream, the profiles relax back onto the upstream profile. It was observed that the profiles obtained at $x/k = 120$ and 200 (not shown) are similar to the upstream profiles. Although none of the velocity scales were able to collapse the profiles in the early region of redevelopment, the mixed scaling does a better job of collapsing the profiles than does the friction velocity.

2. *Reynolds Stresses*

In the redevelopment region, the Reynolds stress profiles attain maxima in the outer layer as far downstream as $x/k = 50$ (Fig. 12). At $x/k = 13$ (not shown) and 21, $\langle u^+u^+\rangle$ exhibits two peaks, which is most distinct in test APG. For example, in test APG (Fig. 12b) at $x/k = 21$, the value of two peaks are $\langle u^+u^+\rangle$ are 25 and 33, and they occurred at $y^+ = 15$ and 185, respectively. Note that the location of the inner peak ($y^+ = 15$) is in the buffer region and is identical to the $y^+ = 15$ reported in canonical boundary layers. Previous studies (Tachie et al. [29] and Le et al. [17]) also made a similar observation in the region of $10 \leq x/k \leq 20$. Nonetheless, they are still several

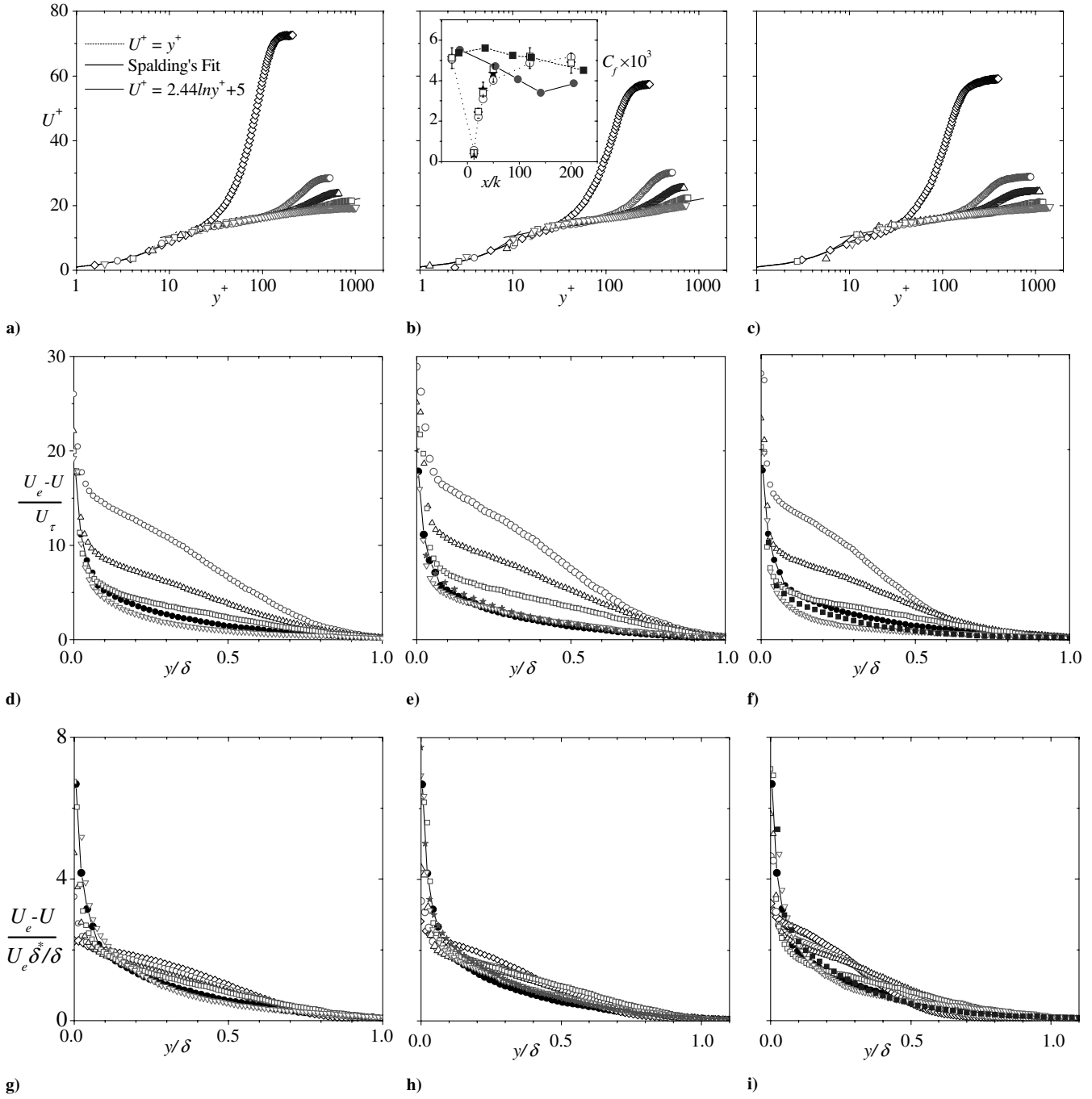

Fig. 11 Mean velocity profiles in inner and outer coordinates: a) CC, b) APG, c) FPG, d) CC, e) APG, f) FPG, g) CC, h) APG, and i) FPG; upstream –●–, $x/k = 13$ ◇, $x/k = 21$ ○, $x/k = 30$ △, $x/k = 50$ □, $x/k = 120$ ▽; reference APG profile at $x/k = 140$ ★ and the FPG profile at $x/k = 123$ ■ is from Shah and Tachie [18].

times larger than the corresponding upstream boundary-layer value. Irrespective of the pressure gradient, the Reynolds stresses are higher than the upstream profiles up to $x/k = 50$. The profiles have nearly recovered to the upstream profile in test CC; however, the presence of the pressure gradient complicated the recovery process. For example, the profiles in test APG and FPG at $x/k = 120$ and 200 (not shown) are self-similar; however, those in test APG are still significantly higher than the corresponding upstream profile, whereas those in test FPG are lower. Because turbulence levels are generally attenuated by FPG and enhanced by APG, these observations imply that in the late stage of flow redevelopment, the pressure gradient becomes the dominant effect. Similar to the findings by Jović [10] in a backward-facing step, the Reynolds stresses recover faster in the inner region than in the outer region (which requires a much longer distance). Furthermore, the profiles obtained in the present APG and FPG experiments are, respectively, higher and lower than the corresponding profiles obtained without a rib on the channel floor.

IV. Conclusions

An experimental study of turbulent flow over a transverse square rib in nearly zero, adverse, and favorable pressure gradients was conducted. The reattachment lengths of $x_r/k = 10.4$, 10.3, and 9.8 were found for the zero, adverse, and favorable pressure gradients, respectively. The mean velocity profiles were distorted substantially downstream of the rib. Similarly, turbulence production was significantly enhanced in the separated shear layer and so were the turbulence intensities and Reynolds shear stress. In the separated region, the convective and diffusion terms in the turbulent kinetic energy transport equation were not negligible so that the production

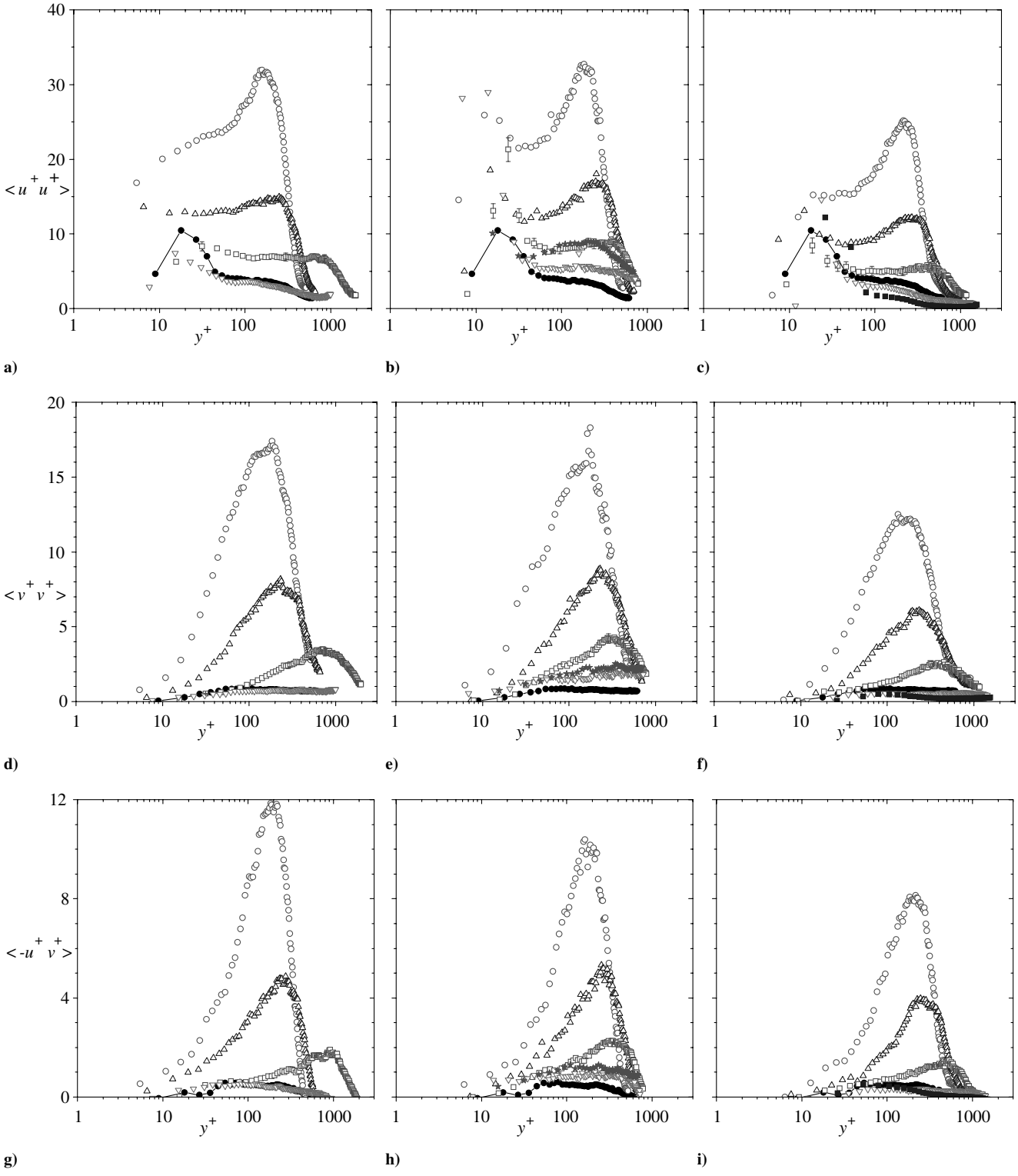

Fig. 12 Reynolds stress profiles: a) CC, b) APG, c) FPG, d) CC, e) APG, f) FPG, g) CC, h) APG, and i) FPG; upstream –●–, $x/k = 21$ ○, $x/k = 30$ △, $x/k = 50$ □, and $x/k = 120$ ▽; reference APG profile at $x/k = 140$ ● and the FPG profile at $x/k = 123$ ■ is from Shah and Tachie [18].

term was not exactly balanced by dissipation rate. Therefore, turbulence models based on equilibrium assumption will not be able to reproduce the flow in the separated region. The flow dynamics in the upper boundary layer of the separated region and early stage of flow redevelopment were insensitive to the pressure gradient. Significant differences were, however, found in the lower boundary layer. For example, the APG modifies the mean velocity and turbulent quantities across a larger portion of the channel than in the FPG. In this region, the mean profiles in the APG increase more gradually from $U = 0$ at the wall to $U_{\max}$ than those in the FPG, whereas the turbulence quantities decay more rapidly from their peak value than those in the APG. Furthermore, APG produced higher mass and momentum deficits than if the pressure gradient were zero or favorable. The results show that the mean defect profiles at various stages of redevelopment collapsed better when scaled with the mixed scaling $U_e\delta^*/\delta$ than when scaled with the friction velocity.

In the nearly zero-pressure-gradient experiments, the profiles of the Reynolds stresses in wall variables became self-similar and collapsed onto the upstream profile at $x/k = 120$. Although the profiles in the adverse and favorable pressure gradients also became

self-similar at $x/k = 120$, they fail to collapse onto the corresponding upstream profiles. In general, the Reynolds stresses in the APG and FPG are, respectively, higher and lower than the upstream profile. Because these are the salient features of APG and FPG flows even without ribs attached to the channel floor, it is concluded that the late stage of flow redevelopment is dominated by the pressure gradient. The results also imply that a significantly longer distance would be required if the APG and FPG flows should ever relax back to the upstream flow. Finally, the profiles obtained in the present FPG channel at $x/k \approx 120$, and those in the same channel but without the ribs, collapsed reasonably well, but significant differences exist between the present and previous data sets in the APG channel.

References

[1] Bradshaw, P., and Wong, F. Y. F., "The Reattachment and Relaxation of a Turbulent Shear Layer," *Journal of Fluid Mechanics*, Vol. 52, No. 1, 1972, pp. 113–135. doi:10.1017/S002211207200299X

[2] Abu-Mulaweh, H. I., "Turbulent Mixed Convection Flow over a Forward-Facing Step—The Effect of Step Height," *International Journal of Thermal Sciences*, Vol. 44, No. 2, 2005, pp. 155–162. doi:10.1016/j.ijthermalsci.2004.08.001

[3] Abdalla, I. E., Cook, M. J., and Yang, Z., "Numerical Study of Transitional Separated-Reattached Flow over Surface-Mounted Obstacles Using Large-Eddy Simulation," *International Journal for Numerical Methods in Fluids*, Vol. 54, No. 2, 2007, pp. 175–206. doi:10.1002/fld.1396

[4] Ruderich, R., and Fernholz, H. H., "An Experimental Investigation of a Turbulent Shear Flow with Separation, Reverse Flow and Reattachment," *Journal of Fluid Mechanics*, Vol. 163, 1986, pp. 283–322. doi:10.1017/S0022112086002306

[5] Kiya, M., and Sasaki, K., "Structure of Turbulent Separation Bubble," *Journal of Fluid Mechanics*, Vol. 137, 1983, pp. 83–113. doi:10.1017/S002211208300230X

[6] Shah, M. K., and Tachie, M. F., "PIV Investigation of Flow over a Transverse Square Rib in Pressure Gradients," 5th AIAA Theoretical Fluid Mechanics Conference, Seattle, WA, AIAA Paper 2008-4347, 2008.

[7] Castro, I. P., and Epik, E., "Boundary Layer Development After a Separated Region," *Journal of Fluid Mechanics*, Vol. 374, 1998, pp. 91–116. doi:10.1017/S0022112098002420

[8] Piirto, M., Saarenrinne, P., Eloranta, H., and Karvinen, R., "Measuring Turbulence Energy with PIV in Backward-Facing Step Flow," *Experiments in Fluids*, Vol. 35, No. 3, 2003, pp. 219–236. doi:10.1007/s00348-003-0607-z

[9] Bergeles, G., and Athanassiadis, N., "The Flow Past a Surface-Mounted Obstacle," *Journal of Fluids Engineering*, Vol. 105, 1983, pp. 461–463.

[10] Jović, S., "Recovery of Reattached Turbulent Shear Layers," *Experimental Thermal and Fluid Science*, Vol. 17, Nos. 1–2, 1998, pp. 57–62. doi:10.1016/S0894-1777(97)10049-8

[11] Djilali, N., and Gartshore, I. S., "Turbulent Flow around a Bluff Rectangular Plate, Part 1: Experimental Investigation," *Journal of Fluids Engineering*, Vol. 113, 1991, pp. 53–59.

[12] Cutler, A. D., and Johnston, J. P., "The Relaxation of a Turbulent Boundary Layer in an Adverse Pressure Gradient," *Journal of Fluid Mechanics*, Vol. 200, 1989, pp. 367–387. doi:10.1017/S0022112089000698

[13] Driver, D. M., and Seegmiller, H. L., "Features of a Reattaching Turbulent Shear Layer in a Divergent Channel Flow," *AIAA Journal*, Vol. 23, No. 2, 1985, pp. 163–171.

[14] Kim, J., Kline, S. J., and Johnston, J. P., "Investigation of a Reattaching Turbulent Shear Layer: Flow over a Backward Facing Step," *Journal of Fluids Engineering*, Vol. 102, 1980, pp. 302–308.

[15] Kuehn, D. M., "Effects of Adverse Pressure Gradient on the Incompressible Reattaching Flow over a Rearward-Facing Step," *AIAA Journal*, Vol. 18, 1980, pp. 343–344.

[16] Ra, S. H., and Chang, P. K., "Effects of Pressure Gradient on Reattaching Flow Downstream of a Rearward-Facing Step," *Journal of Aircraft*, Vol. 27, No. 1, 1990, pp. 93–95.

[17] Le, H., Moin, P., and Kim, J., "Direct Numerical Simulation of Turbulent Flow over a Backward-Facing Step," *Journal of Fluid Mechanics*, Vol. 330, 1997, pp. 349–374. doi:10.1017/S0022112096003941

[18] Shah, M. K., and Tachie, M. F., "PIV Study of Turbulent Flow in Asymmetric Converging and Diverging Channel Flows," *Journal of Fluids Engineering*, Vol. 130, No. 1, 2008, Paper 011204. doi:10.1115/1.2829590

[19] Tachie, M. F., "PIV Study of Turbulent Flow over Transverse Square Ribs in Asymmetric Diffuser," *Physics of Fluids*, Vol. 19, No. 6, 2007, Paper 065106. doi:10.1063/1.2738610

[20] Raffel, M., Willert, C. E., and Kompenhans, J., *Particle Image Velocimetry: A Practical Guide*, Springer, New York, 1998.

[21] Shah, M. K., Agelinchaab, M., and Tachie, M. F., "Influence of PIV Interrogation Area on Turbulent Statistics up to 4th Order Moments in Smooth and Rough Wall Turbulent Flows," *Experimental Thermal and Fluid Science*, Vol. 32, No. 3, 2008, pp. 725–747. doi:10.1016/j.expthermflusci.2007.09.004

[22] Prasad, A. K., Adrian, R. J., Landreth, C. C., and Offutt, P. W., "Effect of Resolution on the Speed and Accuracy of Particle Image Velocimetry Interrogation," *Experiments in Fluids*, Vol. 13, Nos. 2–3, 1992, pp. 105–116. doi:10.1007/BF00218156

[23] Forliti, D. J., Strykowski, P. J., and Debatin, K., "Bias and Precision Errors of Digital Particle Image Velocimetry," *Experiments in Fluids*, Vol. 28, No. 5, 2000, pp. 436–447. doi:10.1007/s003480050403

[24] Coleman, H. W., and Steele, W. G., "Engineering Application of Experimental Uncertainty Analysis," *AIAA Journal*, Vol. 33, 1995, pp. 1888–1896.

[25] Purtell, L. P., Klebanoff, P. S., and Buckley, F. T., "Turbulent Boundary Layer at Low Reynolds Number," *Physics of Fluids*, Vol. 24, 1981, pp. 802–811. doi:10.1063/1.863452

[26] Eaton, J. K., and Johnston, J. P., "A Review of Research on Subsonic Turbulent Flow Reattachment," *AIAA Journal*, Vol. 19, 1981, pp. 1093–1100.

[27] Castro, I. P., "Relaxing Wakes Behind Surface-Mounted Obstacles in Rough Wall Boundary Layers," *Journal of Fluid Mechanics*, Vol. 93, No. 4, 1979, pp. 631–659. doi:10.1017/S0022112079001968

[28] Agelinchaab, M., and Tachie, M. F., "PIV Study of Separated and Reattached Flow Open Channel Flow over Surface Mounted Blocks," *Journal of Fluids Engineering* (to be published).

[29] Tachie, M. F., Balachandar, R., and Bergstrom, D. J., "Open Channel Boundary Layer Relaxation Behind a Forward Facing Step at Low Reynolds Numbers," *Journal of Fluids Engineering*, Vol. 123, No. 3, 2001, pp. 539–544. doi:10.1115/1.1383971

[30] Durst, F., Fischer, M., Jovanovic, J., and Kikura, H., "Methods to Set Up and Investigate Low Reynolds Number, Fully Developed Turbulent Plane Channel Flows," *Journal of Fluids Engineering*, Vol. 120, No. 3, 1998, pp. 496–503. doi:10.1115/1.2820690

[31] Skåre, P. E., and Krogstad, P.-Å., "A Turbulent Equilibrium Boundary Layer Near Separation," *Journal of Fluid Mechanics*, Vol. 272, 1994, pp. 319–348. doi:10.1017/S0022112094004489

[32] Harsha, P. T., and Lee, S. C., "Correlation Between Turbulent Shear Stress and Turbulent Kinetic Energy," *AIAA Journal*, Vol. 8, 1970, pp. 1508–1510.

[33] Launder, B. E., Reece, G. J., and Rodi, W., "Progress in Development of a Reynolds-Stress Turbulence Model Closure," *Journal of Fluid Mechanics*, Vol. 68, No. 3, 1975, pp. 537–566. doi:10.1017/S0022112075001814

[34] Chandrsuda, C., and Bradshaw, P., "Turbulence Structure of a Reattaching Mixing Layer," *Journal of Fluid Mechanics*, Vol. 110, 1981, pp. 171–194. doi:10.1017/S0022112081000670

[35] Jovic, S., "An Experimental Study of a Separated/Reattached Flow Behind a Backward Facing Step, $Re_h = 37,000$," NASA TM 110384, 1996.

[36] Zagarola, M. V., and Smits, A. J., "Mean-Flow Scaling of Turbulent Pipe Flow," *Journal of Fluid Mechanics*, Vol. 373, 1998, pp. 33–79. doi:10.1017/S0022112098002419

[37] Spalding, D. B., "A Single Formula for the Law of the Wall," *Journal of Applied Mechanics*, Vol. 28, 1961, pp. 455–457.

F. Coton
Associate Editor